Macromolecules

ARTICLE

pubs.acs.org/Macromolecules

Triblock Copolymers with Grafted Fluorine-Free, Amphiphilic, Non-Ionic Side Chains for Antifouling and Fouling-Release Applications

Youngjin Cho,[†] Harihara S. Sundaram,[†] Craig J. Weinman,[‡] Marvin Y. Paik,[†] Michael D. Dimitriou,[§] John A. Finlay,[∥] Maureen E. Callow,[∥] James A. Callow,[∥] Edward J. Kramer,[§,⊥] and Christopher K. Ober*[,†]

[†]Department of Materials Science & Engineering, Cornell University, Ithaca, New York 14853, United States

[‡]Intel, CH5-159, Chandler, Arizona 85226, United States

[§]Department of Materials, University of California, Santa Barbara, California 93106, United States

[⊥]Department of Chemical Engineering, University of California, Santa Barbara, California 93106, United States

[∥]School of Biosciences, The University of Birmingham, Birmingham, B15 2TT, U.K.

ABSTRACT: Fluorine-free, amphiphilic, nonionic surface active block copolymers (SABCs) were synthesized through chemical modification of a polystyrene-*block*-poly(ethylene-*ran*-butylene)-*block*-polyisoprene triblock copolymer precursor with selected amphiphilic nonionic Brij and other surfactants. Amphiphilicity was imparted by a hydrophobic aliphatic group combined with a hydrophilic poly(ethylene glycol) (PEG) group-containing moiety. The surfaces were characterized by dynamic water contact angle, atomic force microscopy (AFM), X-ray photoelectron spectroscopy (XPS), and near edge X-ray absorption fine structure (NEXAFS) analysis. In biofouling assays, settlement (attachment) of both spores of the green alga *Ulva* and cells of the diatom *Navicula* on SABCs modified with Brij nonionic side chains was significantly reduced relative to a PDMS standard, with a nonionic surfactant combining a PEG group and an aliphatic moiety demonstrating the best performance. Additionally, a fouling-release assay using sporelings (young plants) of *Ulva* and *Navicula* suggested that the SABC derived from nonionic Brij side chains also out-performed PDMS as a fouling-release material. Good antifouling and fouling-release properties were not demonstrated for the other two amphiphilic surfaces derived from silicone and aromatic group containing nonionic surfactants included in this study. The results suggest that small differences in chemical surface functionality impart more significant changes with respect to the antifouling settlement and fouling-release performance of materials than overall wettability behavior.

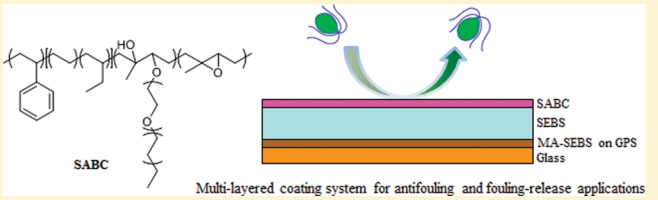

Multi-layered coating system for antifouling and fouling-release applications

INTRODUCTION

Marine biofouling is a worldwide problem caused by the adhesion and accumulation of various marine organisms on a surface immersed in seawater. The economic impact of fouling is mainly a consequence of an increased consumption of fuel and therefore greenhouse gas emissions caused by increased drag.[1,2] Various strategies have been investigated to solve this problem, but to date the most effective have been the use of ablative biocidal coating containing tributyltin (TBT) and copper. Since the global ban on the use of TBT, most antifouling paints are based on copper and organic cobiocides, but these biocidal coatings are also the subject of increasing regulatory scrutiny.[3,4] Consequently, research is currently ongoing to find alternative environmentally benign methods to achieve antifouling and/or fouling-release surfaces.[3,5−8] Additional interest in this area has been generated by the many applications of antifouling surfaces to biomedical devices.[9−12] Two recent reviews have unified these approaches into a coherent discussion of antifouling and fouling-release properties.[13,14]

Because of the wide range of ongoing research, the base of knowledge concerning fouling organisms and methods to deter their settlement and facilitate their release is constantly evolving. A great deal of focus has been on controlling the wettability of coatings through tuning of surface chemistry, with successful antifouling and/or fouling-release behavior demonstrated for both hydrophobic and hydrophilic coatings. Hydrophobic poly(dimethylsiloxane) (PDMS) coatings have demonstrated excellent fouling-release properties as a result of their low surface energy in conjunction with their low modulus and elasticity,[15−17] and there is currently a lot of research focused on improving performance.[18−20] Other promising hydrophobic coatings for fouling control applications have included perfluorinated polyether based random terpolymers and poly(styrene)-*block*-poly(isoprene) block copolymers containing fluorinated side chains.[21] A recent review paper describes the role of block copolymer microstructure in fouling release applications.[22] Hydrophilic coatings for fouling prevention meanwhile have generally focused on either the use of poly(ethylene

Received: February 6, 2011
Revised: April 28, 2011
Published: May 24, 2011

glycol) (PEG), known for its exceptional resistance to protein adsorption and cell adhesion,[23−25] in various applications. Zwitterionic materials have also demonstrated exceptional fouling resistance.[26−29]

However, a recent study documented a limitation in pursuing a strictly hydrophobic or hydrophilic approach to marine fouling control. Krishnan et al. profiled the fouling settlement and release of two complementary ubiquitous types of marine algae against a range of hydrophobic and hydrophilic coating surfaces.[30] While hydrophilic block copolymer coatings containing PEG side chains were found to perform extremely well with respect to the release of diatoms (unicellular algae that form slimes), hydrophobic fluorinated block copolymer and PDMS coatings were found to perform much better with respect to removal of sporelings of the green alga *Ulva*. Thus, much recent work has focused on the production of ambiguous amphiphilic coatings able to present both hydrophobic and hydrophilic moieties at the surface. Gudipati et al. produced hyperbranched polymers containing both fluorinated and PEGylated groups that achieved both low protein adsorption and high fouling release at an optimal composition of hydrophobic and hydrophilic monomers.[31] More recently, Ober and co-workers reported the development of several surface active block copolymers with amphiphilic side chains derived from a nonionic ethoxylated fluorosurfactant capable of both resisting and releasing *Ulva* and the diatom *Navicula*, and also deterring barnacle settlement.[32−34] Additionally, similar fluorinated side chain surface active block copolymers reported by Martinelli et al. also demonstrated exceptional fouling release properties with regards to marine algal fouling.[35] These results clearly demonstrate the potential of using amphiphilic coatings to combat marine fouling. All the systems described relied on fluorinated moieties to impart hydrophobicity to the amphiphilic system. However, the recent finding that fluorinated compounds with more than four consecutive CF_2 units are potentially environmental hazards[36,37] requires the creation of alternative materials with similar outstanding characteristics.

Therefore, this study reports the synthesis, characterization, and biofouling performance of surface active block copolymers (SABCs) derived from the grafting of various fluorine-free, nonionic side chains to a specially designed polystyrene-*block*-poly(ethylene-*ran*-butylene)-*block*-poly(isoprene) (PS-*b*-P(E/B)-*b*-PI, K3) triblock precursor copolymer. Surfaces were challenged with spores of the green alga *Ulva* and cells of the diatom *Navicula* to test their resistance to biofouling and ease with which these marine organisms can be removed (fouling-release). Surface characteristics of the resultant SABCs were determined using dynamic water contact angle, atomic force microscopy (AFM), X-ray photoelectron spectroscopy (XPS), near edge X-ray absorption fine structure (NEXAFS) analysis.

EXPERIMENTAL SECTION

Materials. The polystyrene$_{8K}$-*block*-poly(ethylene-*ran*-butylene)$_{25K}$-*block*-polyisoprene$_{10K}$ (PS_{8K}-*b*-P(E/B)$_{25K}$-*b*-PI_{10K}) triblock precursor copolymer (K3) was produced using anionic polymerization and subsequent catalytic hydrogenation by Kraton Polymers at large scale (∼0.5 kg) to facilitate preparation of SABCs. 3-Chloroperoxybenzoic acid (*m*-CPBA, ClC_6H_4COOOH, FW 172.57, 77%), boron trifluoride diethyl etherate (BF_3•Et_2O, BF_3•$O(CH_2CH_3)_2$, FW 141.93, 99.9%), Brij 56 (registered trademark of Croda International PLC, $CH_3(CH_2)_{15}(OCH_2CH_2)_nOH$, $n \sim 10$, $M_n \approx 683$), Tergitol NP-9 (registered trademark of Union Carbide Chemicals and Plastics Technology Corporation, $CH_3(CH_2)_8C_6H_4(OCH_2CH_2)_9OH$, FW 616.82), poly(ethylene glycol) butyl ether, Brij 30, Brij 72, Brij 76, Brij 78, and Brij 97, and anhydrous chloroform ($CHCl_3$) were purchased from Sigma-Aldrich and used as received with no further purification. Silwet L-408 ($[(CH_3)_3SiO]_2CH_3Si(CH_2)_3(OCH_2CH_2)_nOH$, $n \sim 11$, $M_n \approx 720$) was generously provided by Momentive Performance Materials and used as received. Cyclohexane, dichloromethane (CH_2Cl_2), methanol (CH_3OH), toluene, 6.25 N sodium hydroxide (NaOH), 96% sulfuric acid (H_2SO_4), 30 wt % hydrogen peroxide (H_2O_2) in water, 95% ethanol (CH_3CH_2OH), and all other reagents were used as received. 3-(Glycidoxypropyl)trimethoxysilane (GPS, 99%) was purchased from Gelest and used as received. Polystyrene-*block*-poly(ethylene-*ran*-butylene)-*block*-polystyrene (SEBS) triblock thermoplastic elastomers (Kraton MD6945) and SEBS grafted with maleic anhydride (MA-SEBS, Kraton FG1901X) were generously provided by Kraton Polymers.

Synthesis of Epoxidized PS_{8K}-*b*-P(E/B)$_{25K}$-*b*-PI_{10K}. The PS_{8K}-*b*-P(E/B)$_{25K}$-*b*-PI_{10K} SABC precursor polymer (5 g, 14.5 mmol of reactive isoprene sites) was dissolved in 100 mL of cyclohexane in a round bottomed flask. 3-Chloroperoxybenzoic acid (*m*-CPBA, 3.9 g, 17.4 mmol) was added to the mixture, and the solution was stirred vigorously for 5 h at room temperature. Subsequently, the polymer was precipitated in methanol, collected by filtration, and reprecipitated from dichloromethane to remove residual *m*-CPBA and its respective byproducts. The white, rubbery product was dried at room temperature under reduced pressure for 48 h to remove remaining solvent. ^{1}H NMR for epoxidized PS_{8K}-*b*-P(E/B)$_{25K}$-*b*-PI_{10K} (300 MHz, $CDCl_3$, δ): 6.58, 7.10, (5H, styrene), 2.68 (br s, 1H, epoxidized isoprene, $-CH_2HCOC(CH_3)CH_2-$), 0.80, 1.08, 1.26, 1.47, 1.57 (backbone). IR (dry film) υ_{max} (cm^{-1}): 2925, 2850 (C−H stretching); 1470 (C−H bending); 1070 (C−O stretching); 880 (C−O−C stretching); 700 (C−H bending, aromatic).

Synthesis of the Surface Active Block Copolymers with Grafted Amphiphilic, Nonionic Side Chains. To produce ether-linked side chain surface active block copolymers, 2.1 g of epoxidized PS_{8K}-*b*-P(E/B)$_{25K}$-*b*-PI_{10K} (5.8 mmol of epoxide) was taken in a round-bottomed flask in conjunction with a 3-fold molar excess (17.4 mmol) of side chain precursor nonionic surfactant alcohols. The reactants were purged with argon, and subsequently dissolved in 150 mL of anhydrous chloroform. Activated molecular sieves were added to the reaction mixture and it was allowed to sit for 12 h to optimize the adsorption of water. Etherification was performed through the addition of boron trifluoride diethyl etherate catalyst (0.345 g, 2.4 mmol) followed by vigorous stirring at room temperature for 48 h. Following the reaction, 1 mL of 6.25 N sodium hydroxide aqueous solutions was added to quench any residual boron catalyst and the reaction mixture was concentrated under reduced pressure using a rotary evaporator. The resultant surface active triblock copolymers were precipitated into methanol. The SABCs were collected by filtration and subsequently reprecipitated twice into methanol from chloroform to remove additional residual surface active side-chain alcohol precursors. Finally, the finished compounds were dried under reduced pressure at room temperature for 48 h to fully remove residual solvent. ^{1}H NMR for PS_{8K}-*b*-P(E/B)$_{25K}$-*b*-PI_{10K} functionalized with Brij 56 side chains (300 MHz, $CDCl_3$, δ): 6.58, 7.10 (5H, styrene); 3.65 (br s, 40H, $-(OCH_2CH_2)_{10}-$); 3.43 (t, 2H, $-(CH_2CH_2O)_{10}CH_2(CH_2)_{14}-$); 0.82, 1.06, 1.24, 1.82 (31H, $CH_3(CH_2)_{14}CH_2-$ of Brij 56 side chain, and backbone). IR (dry film) υ_{max} (cm^{-1}): 3480 (O−H stretching); 2930, 2855 (C−H stretching); 1460, 1380 (C−H bending); 1115 (C−O stretching); 765, 700 (C−H bending, aromatic). ^{1}H NMR for PS_{8K}-*b*-P(E/B)$_{25K}$-*b*-PI_{10K} functionalized with Tergitol NP-9 side chains (300 MHz, $CDCl_3$, δ): 6.56, 6.84, 7.10 (5H, styrene; 4H, Tergitol NP-9 side chain); 4.10 (t, 2H, $-C_6H_4OCH_2CH_2O-$); 3.85 (t, 2H, $-C_6H_4OCH_2CH_2O-$); 3.66 (br m, $-C_6H_4OCH_2CH_2(OCH_2CH_2)_8-$); 0.84, 1.06, 1.24, 1.75 (19H, $CH_3(CH_2)_8-$ of Tergitol NP-9 side chain, and backbone). IR (dry film)

υ_{max} (cm^{-1}): 3510 (O−H stretching); 2925, 2860 (C−H stretching); 1460, 1380 (C−H bending); 1120 (C−O stretching); 770, 700 (C−H bending, aromatic). ^{1}H NMR for PS_{8K}-*b*-$P(E/B)_{25K}$-*b*-PI_{10K} functionalized with Silwet L-408 side chains (300 MHz, $CDCl_3$, δ): 6.58, 7.08 (5H, styrene), 3.65 (br s, 44H, -$(OCH_2CH_2)_{11}$−); 3.40 (t, 2H, −$(CH_2)_2CH_2(OCH_2CH_2)_{11}$−); 0.83, 1.06, 1.25, 1.81 (backbone), 0.43 (m, 2H, $[(CH_3)_3SiO]_2CH_3SiCH_2(CH_2)_2$−); 0.08 (br s, 18H, $[(CH_3)_3SiO]_2CH_3Si(CH_2)_3$−); 0.00 (s, 3H, $[(CH_3)_3SiO]_2CH_3$-$Si(CH_2)_3$−). IR (dry film) υ_{max} (cm^{-1}): 3480 (O−H stretching); 2925, 2855 (C−H stretching); 1460, 1360 (C−H bending); 1110 (C−O stretching); 765, 700 (C−H bending, aromatic). ^{1}H NMR for PS_{8K}-*b*-$P(E/B)_{25K}$-*b*-PI_{10K} functionalized with poly(ethylene glycol)butyl ether side chains (300 MHz, $CDCl_3$, δ): 6.58, 7.09 (5H, styrene), 3.66 (br s, 16H, −$(OCH_2CH_2)_4$−); 3.46 (t, 2H, −$(CH_2CH_2O)_4CH_2(CH_2)_2$−); 0.80, 0.91, 1.07, 1.25, 1.34, 1.57 (7H, $CH_3(CH_2)_2CH_2$− of poly(ethylene glycol)butyl ether side chain, and backbone). Anal. Found: C, 77.70; H, 11.62; O, 10.68. ^{1}H NMR for PS_{8K}-*b*-$P(E/B)_{25K}$-*b*-PI_{10K} functionalized with Brij 30 side chains (300 MHz, $CDCl_3$, δ): 6.52, 7.05 (5H, styrene), 3.65 (br s, 16H, −$(OCH_2CH_2)_4$−); 3.42 (t, 2H, −$(CH_2CH_2O)_4CH_2(CH_2)_{10}$−); 0.80, 1.02, 1.21, 1.51, 1.79 (23H, $CH_3(CH_2)_{10}CH_2$− of Brij 30 side chain, and backbone). Anal. Found: C, 78.67; H, 11.75; O, 9.58. ^{1}H NMR for PS_{8K}-*b*-$P(E/B)_{25K}$-*b*-PI_{10K} functionalized with Brij 72 side chains (300 MHz, $CDCl_3$, δ): 6.58, 7.09 (5H, styrene), 3.65 (br s, 40H, −$(OCH_2CH_2)_{10}$−); 3.44 (t, 2H, −$(CH_2CH_2O)_{10}CH_2(CH_2)_{16}$−); 0.82, 1.07, 1.25, 1.84 (35H, CH_3-$(CH_2)_{16}CH_2$− of Brij 72 side chain, and backbone). Anal. Found: C, 78.97; H, 11.93; O, 9.10%. ^{1}H NMR for PS_{8K}-*b*-$P(E/B)_{25K}$-*b*-PI_{10K} functionalized with Brij 76 side chains (300 MHz, $CDCl_3$, δ): 6.58, 7.09 (5H, styrene), 3.64 (br s, 40H, −$(OCH_2CH_2)_{10}$−); 3.44 (t, 2H, −$(CH_2CH_2O)_{10}CH_2(CH_2)_{16}$−); 0.82, 1.07, 1.25, 1.81 (35H, CH_3-$(CH_2)_{16}CH_2$− of Brij 76 side chain, and backbone). Anal. Found: C, 76.43; H, 11.57; O, 12.00. ^{1}H NMR for PS_{8K}-*b*-$P(E/B)_{25K}$-*b*-PI_{10K} functionalized with Brij 78 side chains (300 MHz, $CDCl_3$, δ): 6.52, 7.04 (5H, styrene), 3.53 (br s, 80H, −$(OCH_2CH_2)_{20}$−); 3.39 (t, 2H, −$(CH_2CH_2O)_{20}CH_2(CH_2)_{16}$−); 0.82, 1.01, 1.20, 1.52, 1.79 (35H, $CH_3(CH_2)_{16}CH_2$− of Brij 78 side chain, and backbone). Anal. Found: C, 73.52; H, 11.24; O, 15.24. ^{1}H NMR for PS_{8K}-*b*-$P(E/B)_{25K}$-*b*-PI_{10K} functionalized with Brij 97 side chains (300 MHz, $CDCl_3$, δ): 6.58, 7.10 (5H, styrene), 5.34 (m, 2H, −CH═CH− of Brij 97 side chain); 3.64 (br s, 40H, −$(OCH_2CH_2)_{10}$−); 3.44 (t, 2H, −$(CH_2CH_2O)_{10}CH_2$-$(CH_2)_{16}$−); 2.01(m, 4H, −CH_2−CH═CH−CH_2−); 0.82, 1.07, 1.25, 1.82 (27H, $CH_3(CH_2)_6CH_2$− and −$(CH_2CH_2O)_{10}CH_2(CH_2)_6$-$CH_2$− of Brij 97 side chain, and backbone). Anal. Found: C, 74.67; H, 11.32; O, 14.85.

Measurements. ^{1}H NMR spectra were recorded using a Varian Gemini spectrometer with deuterated chloroform. The FTIR spectra of the polymers cast as films from tetrahydrofuran (THF) solution on sodium chloride plates was collected using a Mattson 2020 Galaxy Series FTIR spectrometer. Elemental analysis for weight percent C, H, and O of the surface active block copolymers was performed by Quantitative Technologies, Inc. (QTI). Gel permeation chromatography (GPC) of a THF solution of polymers (1 mg/mL) was carried out using four Waters Styragel HT columns operating at 40 °C in conjunction with Waters 490 ultraviolet (λ = 254 nm) and Waters 410 refractive index detectors. The molecular weight range of the columns was from 500 to 10^7 g/mol. THF was used as the eluent at a flow rate of 1 mL/min, and toluene was used as a marker for flow calibration. The GPC was calibrated using a series of low-dispersity polystyrene standards.

Water contact angles were measured using a contact angle goniometer (AST Products, Inc. model VCA Optima XE) at room temperature. Dynamic water contact angle measurements were performed through the addition and retraction of a small drop of water (2 μL) on the surface. The advancing and receding contact angle behavior was digitally recorded and image analysis software was used to measure the angles. Three measurements each for two different areas on the surface were taken.

Tapping-mode AFM measurements were made using a Digital Instruments Dimension 3000 atomic force microscope. Phase-contrast images were collected over 1 μm × 1 μm regions to reveal the surface morphology. Images were collected using Applied Nanostructures long cantilevers (ACL) at 1.5 Hz. Tapping was sufficiently hard to tap through the soft surface layer of the ethylene-butylene block.

XPS measurements were performed using a Kratos Axis Ultra Spectrometer (Kratos Analytical, Manchester, U.K.) with a monochromatic Al Kα X-ray source (1486.6 eV) operating at 225 W under a vacuum of 1.0 × 10^{-8} Torr. Charge compensation was carried out by injection of low-energy electrons into the magnetic lens of the electron spectrometer. The pass energy of the analyzer was set at 40 eV for high-resolution spectra and 80 eV for survey scans, with energy resolutions of 0.05 and 1 eV, respectively. The spectra were analyzed using Casa XPS v.2.3.12Dev4 software. The C−C peak at 285 eV was used as the reference for binding energy calibration.

Near edge X-ray absorption fine structure (NEXAFS) measurements were carried out on the U7A NIST/Dow materials characterization endstation at the National Synchrotron Light Source at Brookhaven National Laboratory (BNL). The general underlying principles of NEXAFS and a description of the beamline at BNL have been previously reported.[38,39] The X-ray beam was elliptically polarized (polarization factor = 0.85), with the electric field vector dominantly in the plane of the storage ring. The photon flux was approximately 1 × 10^{11} photons per second at a typical storage ring current of 750 mA. A spherical grating monochromator was used to obtain monochromatic soft X-rays at an energy resolution of 0.2 eV. The C 1s NEXAFS spectra were acquired for incident photon energy in the range of 270−320 eV. The angle of incidence of the X-ray beam, measured from the sample surface, was varied. The partial-electron-yield (PEY) signal was collected using a channeltron electron multiplier with an adjustable entrance grid bias (EGB). Data were reported for a grid bias of −150 V. The channeltron PEY detector was positioned at an angle of 35° above the equatorial plane of the sample chamber and at an angle of 36° in that plane relative to the incoming X-ray beam.[40] The PEY C 1s spectra were normalized by subtracting a linear pre-edge baseline and setting the edge jump to unity at 320 eV. The photon energy was calibrated by adjusting the peak position of the lowest π^* phenyl resonance from polystyrene to 285.5 eV.

Preparation of Surfaces for Surface Characterization and Biofouling Assays. Surfaces for dynamic water contact angle analysis, XPS, NEXAFS, AFM, and biofouling assays were prepared on silicon wafers by spin-coating and glass slides by spray-coating. The silicon wafers were prepared by spin-coating 3% (w/v) solutions of SABCs in toluene at 2000 rpm for 60 s. The spin-coated silicon wafers were annealed in a vacuum oven at reduced pressure at 120 °C for 12 h followed by slow cooling to room temperature. The spray-coated glass slides were prepared as previously reported.[41] The glass slides were cleaned by immersion in a 7:3 (v/v) mixture of concentrated H_2SO_4 and 30 wt % H_2O_2 solution, and then rinsed well with water, dried, and subsequently functionalized with a 4%(w/v) solution of 3-(glycidoxy)trimethoxysilane in ethanol. The silane was cured by heating the functionalized glass slides to 110 °C for 2 h followed by slow cooling to room temperature. This epoxy-containing silane served as an adhesion promoter for the initial SEBS layer spin coated from a 7% w/v SEBS solution in toluene (5% Kraton FG-1901X or 2% MD 6945). The thickness of the SEBS base layer was then built up through successive spin coating of a 12% w/v SEBS solution (Kraton MD 6945) in toluene three times. It has been demonstrated that an elastomer layer is needed for efficient removal of hard foulers such as barnacles.[45] Finally, a relatively thin layer of SABC was deposited on top of the SEBS base layer through spray coating from a 3% w/v

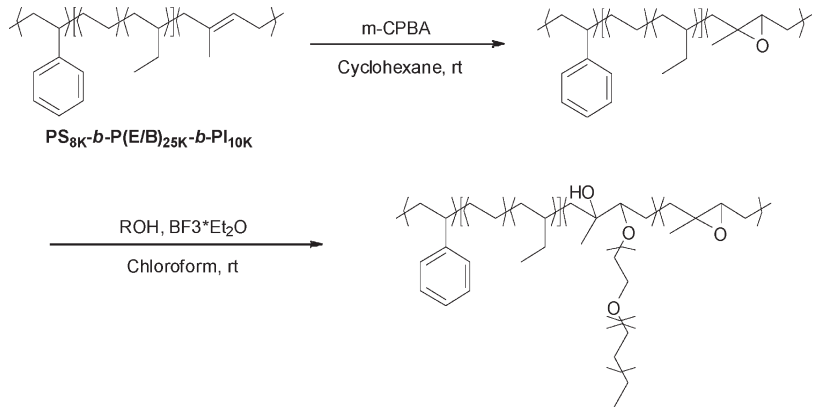

Figure 1. Synthesis of the surface active triblock copolymer with grafted nonionic amphiphilic side chains. ROH = $CH_3(CH_2)_8C_6H_4(OCH_2CH_2)_9OH$ (Tergitol NP-9), or $[(CH_3)_3SiO]_2CH_3Si(CH_2)_3(OCH_2CH_2)_n$ OH, $n \sim 11$ (Silwet L-408). ROH = $C_mH_{2n+1}(OCH_2CH_2)_nOH$ [($m = 4$, $n \sim 4$), ($m = 12$, $n \sim 4$), ($m = 16$, $n \sim 10$), ($m = 18$, $n \sim 2$), ($m = 18$, $n \sim 10$), ($m = 18$, $n \sim 20$)]; $C_mH_{2n-1}(OCH_2OCH_2)_nOH$ ($m = 18$, $n \sim 20$).

solution in toluene. The glass slides were annealed at 60 °C for 24 h and 120 °C for 24 h. The SEBS base-layer thickness produced was on the order of ~500 μm. Meanwhile, the SABC layer deposited onto the SEBS base layer via spray coating produced a layer on the order of ~20 μm in thickness.

A poly(dimethylsiloxane) elastomer (PDMSe) (Silastic T2; Dow Corning), known to possess good fouling-release properties against *Ulva*, and prepared as described by Schumacher et al.,[42] was included in the release assays as a standard. Kraton MD6945 was used as the thermoplastic elastomer base layer in the multilayer coating to produce an under layer with a relatively low Young's modulus that has been shown to be important for the best fouling-release performance.[34] MD 6945 SEBS and PS_{8K}-*b*-$P(E/B)_{25K}$-*b*-PI_{10K} triblock precursor copolymer (K3) were also included as controls.

Settlement of Zoospores and Strength of Attachment of Sporelings of *Ulva*. Nine replicate test samples were immersed in a 30 L tank of recirculating deionized water at ~20 °C for 48 h. The slides were equilibrated in artificial seawater 1 h prior to the start of the experiments. Zoospores were released from fertile plants of *Ulva* linza and prepared for assay as described previously.[43] Then 10 mL aliquots of zoospore suspension (1×10^6 spores per mL), were pipetted into individual compartments of Quadriperm polystyrene culture dishes (Greiner Bio-One), each containing a test slide. The test slides were incubated in the dark at ~20 °C for 1 h and gently washed in seawater to remove zoospores that had not settled. Three slides were fixed using 2.5% glutaraldehyde in seawater and these replicates were used to quantify the density of zoospores attached to the surfaces as previously reported.[44]

Sporelings of *Ulva* (young plants) were cultured on 6 replicates of each coating.[45] After washing, the samples were transferred to dishes containing nutrient enriched seawater for 7 days. Growth was estimated by direct measurement of fluorescence from chlorophyll contained within the chloroplasts of the sporelings using a Tecan plate reader (GENios Plus).[46] Fluorescence was recorded as Relative Fluorescence Units (RFU) from direct readings. The slides (6 replicates) were read from the top, 70 readings per slide, taken from the central 25 cm^2. The strength of attachment of the sporelings was determined by jet washing using a water jet.[47] The range of impact pressures used was chosen to provide maximum information on the strength of attachment of the sporelings. After exposure to the water jet, RFU readings were again taken from the central part of the slide. Percentage removal was calculated from the mean RFU reading before and after exposure to the water jet. From curves of the percentage removal vs impact pressure, the critical water pressure (kPa) required to remove 50% of the sporelings was derived.

Attachment and Adhesion Strength of Cells of the Diatom *Navicula*. Cells of *Navicula* were cultured in F/2 medium contained in 250 mL conical flasks. A long-phase suspension of cells was diluted to give a suspension with a chlorophyll content of approximately 0.25 μg/mL. Ten milliliters of cell suspension was added to individual compartments of Quadriperm polystyrene culture dishes (Greiner Bio-One), each containing a test slide. After 2 h at 20 °C on the laboratory bench, the slides were gently washed in seawater without exposure to air (i.e., a submerged wash) to remove cells that had not attached to the surface. Cells on 3 replicate slides of each coating type were fixed and counted as described for spores of *Ulva*. To determine the strength of attachment, a further 3 replicate slides were exposed to a wall shear stress of 23 Pa in a calibrated water channel prior to fixation. The percentage removal of cells was calculated by comparing cell counts on slides not exposed to shear with those on slides after exposure to shear.

RESULTS AND DISCUSSION

Polymer Synthesis and Characterization. The fluorine-free, amphiphilic surface active block copolymers were produced through a straightforward two step modification of the PS_{8K}-*b*-$P(E/B)_{25K}$-*b*-PI_{10K} precursor polymer depicted in Figure 1, in a similar fashion to that previously reported by Weinman et al.[34] Functionalization of the PI block of the triblock precursor was achieved through epoxidation of the residual alkene groups followed by subsequent catalytic ring-opening etherification reactions using nonionic surfactant alcohols carrying amphiphilic functionality.

The synthesis of fluorine-free, nonionic, side chain-derived amphiphilic SABCs was monitored using both FTIR spectroscopy and ^{1}H NMR spectroscopy. Following the epoxidation reaction, ^{1}H NMR spectroscopy clearly showed that there was no longer evidence of any alkene protons, and a significant peak at ~2.7 ppm appeared indicating the presence of protons adjacent to the newly formed oxirane rings on the PI backbone. Additionally, FTIR spectroscopy clearly showed the appearance of a C−O−C stretching peak at roughly 880 cm^{-1} associated with the epoxide ring. The C═C absorption at 960 cm^{-1} disappeared. This indicated that all of the residual unsaturated alkene groups were successfully converted to their epoxidized form. Subsequent catalytic ring-opening using nonionic surfactant alcohols led to the disappearance of the epoxide peak in the ^{1}H NMR spectra. Further analysis of the ^{1}H NMR spectra demonstrated the appearance of peaks at ~3.6 and 3.4 ppm indicating the presence

Table 1. Percent Attachment of Non-Ionic Surfactant Side Chains Relative to Epoxy in the Precursor Polymer, PDI, the Measured Advancing ($\theta_{w,ad}$) and Receding Water Contact Angles ($\theta_{w,re}$), and the Binding Energy (eV) in XPS for Each Surface

					binding energy(eV) in XPS		
block copolymer	attachment (%)	PDI	$\theta_{w,ad}$ (deg)	$\theta_{w,re}$ (deg)	C 1s	O 1s	Si 2p
PS_{8K}-*b*-$P(E/B)_{25K}$-*b*-PI_{10K}-Brij 56	18	1.2	102 ± 3	25 ± 2	285	535	
PS_{8K}-*b*-$P(E/B)_{25K}$-*b*-PI_{10K}-Tergitol NP-9	50	1.3	108 ± 3	22 ± 1	285	535	
PS_{8K}-*b*-$P(E/B)_{25K}$-*b*-PI_{10K}-Silwet L-408	26	1.6	107 ± 2	22 ± 3	285	535	100/150

Table 2. Attachment, PDI, and Elemental Analysis of the Triblock Copolymer with Grafted Brij Non-Ionic Amphiphilic Side Chains

				elemental analysis		
block copolymer	ROH (SABC)	attachment (%)	PDI	% C	% H	% O
PS_{8K}-*b*-$P(E/B)_{25K}$-*b*-PI_{10K}-PEG.BE	$C_4H_9(OCH_2CH_2)_nOH$, $n \sim 4$	40.00	1.55	77.70	11.62	10.68
PS_{8K}-*b*-$P(E/B)_{25K}$-*b*-PI_{10K}-Brij 30	$C_{12}H_{25}(OCH_2CH_2)_4OH$	36.53	1.48	78.67	11.75	9.58
PS_{8K}-*b*-$P(E/B)_{25K}$-*b*-PI_{10K}-Brij 72	$C_{18}H_{37}(OCH_2CH_2)_nOH$, $n \sim 2$	45.71	1.29	78.97	11.93	9.10
PS_{8K}-*b*-$P(E/B)_{25K}$-*b*-PI_{10K}-Brij 76	$C_{18}H_{37}(OCH_2CH_2)_nOH$, $n \sim 10$	37.63	1.24	76.43	11.57	12.00
PS_{8K}-*b*-$P(E/B)_{25K}$-*b*-PI_{10K}-Brij 78	$C_{18}H_{37}(OCH_2CH_2)_nOH$, $n \sim 20$	28.46	1.16	73.52	11.24	15.24
PS_{8K}-*b*-$P(E/B)_{25K}$-*b*-PI_{10K}-Brij 97	$C_{18}H_{35}(OCH_2CH_2)_nOH$, $n \sim 10$	35.48	1.68	74.67	11.32	14.85

of oligoethylene glycol groups for the Brij functionalized triblock copolymers, indicating successful attachment of the amphiphilic side chain. For the Tergitol NP-9 block copolymer, similar peaks for the oligoethylene glycol groups of the side chain were seen at ~4.1, 3.9, and 3.7 ppm, in addition to the appearance of a third aromatic proton peak at ~6.8 ppm corresponding to the aromatic protons of the Tergitol NP-9 side chain. Finally, the Silwet L-408 block copolymer showed oligoethylene glycol protons at ~3.6 and 3.4 ppm, but additional peaks at 0.43 and 0.08 ppm were present from the $-CH_3$ groups attached to Si atoms present in the side chain. These findings were supported by FTIR spectroscopy which demonstrated the appearance of a strong O−H stretching peak between 3300 and 3500 cm^{-1}, formed during ring-opening of the epoxy, and a C−O stretching peak at ~1115 cm^{-1}, formed from the etherification attachment of side chains, for all triblock copolymers.

Table 1 demonstrates the characterizations of three of the nonionic surfactants relative to epoxy functionality in the epoxidized PS-*b*-P(E/B)-*b*-PI precursor. The percentage of nonionic surfactant successfully attached was calculated by integration of ^1H NMR spectra. Specifically, this value was obtained by comparing the total amount of aromatic protons (associated with the PS block, or in the case of Tergitol NP-9, the PS block and the attached side chain) in the ^1H NMR spectra with the number of protons associated with the PEG part of the amphiphilic, nonionic, surfactant-derived side chain. The percent attachment of side chain relative to the amount of epoxy groups in the PS_{8K}-*b*-$P(E/B)_{25K}$-*b*-PI_{10K} precursor was found to be 18% for Brij 56, 50% for Tergitol NP-9, and 26% for Silwet L-408. Using GPC, the dispersity index (PDI) of the triblock copolymer was found to increase from 1.06 for the PS-*b*-P(E/B)-*b*-PI precursors to 1.12 when epoxidized. Finished, substituted SABC containing Brij 56 and Tergitol NP-9 side chains generally had a PDI between 1.2 and 1.3. The SABC produced from Silwet L-408 experienced a rise in PDI to 1.6. This rise in PDI for all SABCs combined with the observation of complete reaction of the epoxide despite less than 100% attachment of nonionic surfactant side chain suggests that some of the epoxide was most likely lost to intermolecular cross-linking reactions between epoxide rings. Additionally, intramolecular reactions in combination with epoxide ring-opening by any residual water molecules left in the reaction mixture may have contributed to this relatively low observed attachment. The additional increase in PDI for the Silwet L-408 SABC suggests that an additional undesirable side reaction likely enhanced cross-linking. Dynamic water contact angle analysis of SABCs indicated the presence of low surface energy, hydrophobic moieties at the surface for all three side chain polymers with $\theta_{w,advancing}$ ranging from 102° to 108°. High contact angle hysteresis was seen for all three samples, with $\theta_{w,receding}$ measured between 22° and 25°, suggesting the facile reordering of the side chains to orient the hydrophilic PEG groups at the surface. It was notable that both advancing and receding water contact angle measurements for all three samples were not statistically different, demonstrating that all three nonionic side chains derived SABCs had very similar wettability characteristics. Analysis of the XPS survey scans show all surfaces dominated by the peaks associated with C 1s and O 1s, located at 285 and 535 eV respectively. Additionally, Si 2p peaks at 150 and 100 eV were present in the amphiphilic SABC derived from the PS_{8K}-*b*-$P(E/B)_{25K}$-*b*-PI_{10K} precursor with attached Silwet L-408 nonionic side chains, due to the presence of Si in the Silwet L-408 side chain.

Table 2 shows the percentage of attachment of various Brij nonionic side chains relative to epoxy functionality in the epoxidized PS-*b*-P(E/B)-*b*-PI precursor, PDI, and elemental analysis of the triblock copolymer with grafted amphiphilic, nonionic Brij side chains. The aim of this study was to examine systemically the effects of PEG and aliphatic unit length on nonionic Brij side chains. The percent attachment of side chain in the PS_{8K}-*b*-$P(E/B)_{25K}$-*b*-PI_{10K} precursor was found to be 40.00% for PEGBE, 36.53% for Brij 30, 45.71% for Brij 72, 37.63% for Brij 76, 28.46% for Brij 78, and 35.48% for Brij 97. The dispersity index of the triblock copolymers was found between 1.16 and 1.68.

Table 3. Water Contact Angles of the Triblock Copolymer Surface with Grafted Amphiphilic, Non-Ionic Brij Side Chains

surface	no. of aliphatic units:EO units	$\theta_{w,ad}$ (deg)	$\theta_{w,re}$ (deg)	hysteresis
SEBS	-	119.8 ± 3.2	59.8 ± 3.9	60.0
PS_{8K}-*b*-$P(E/B)_{25K}$-*b*-PI_{10K} (K3)	-	115.9 ± 1.2	57.6 ± 1.5	58.3
PS_{8K}-*b*-$P(E/B)_{25K}$-*b*-PI_{10K}-PEG.BE	4:4	103.6 ± 3.1	28.7 ± 0.7	74.9
PS_{8K}-*b*-$P(E/B)_{25K}$-*b*-PI_{10K}-Brij 30	12:4	107.9 ± 1.2	24.9 ± 0.6	83.0
PS_{8K}-*b*-$P(E/B)_{25K}$-*b*-PI_{10K}-Brij 72	18:2	109.6 ± 1.6	26.6 ± 1.8	83.0
PS_{8K}-*b*-$P(E/B)_{25K}$-*b*-PI_{10K}-Brij 76	18:10	98.5 ± 2.6	18.1 ± 3.2	80.4
PS_{8K}-*b*-$P(E/B)_{25K}$-*b*-PI_{10K}-Brij 78	18:20	84.1 ± 2.3	16.9 ± 2.7	67.2
PS_{8K}-*b*-$P(E/B)_{25K}$-*b*-PI_{10K}-Brij 97	18[a]:10	105.3 ± 1.8	22.4 ± 1.7	82.9

[a] Unsaturated.

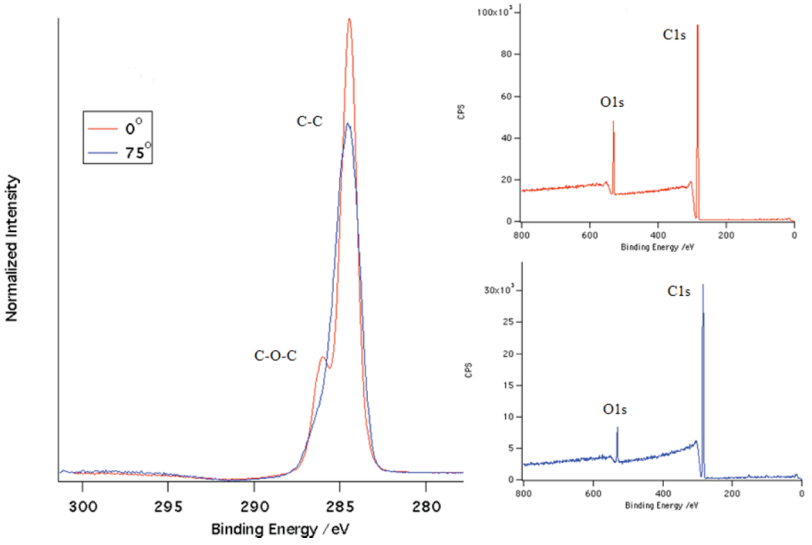

Figure 2. XPS of the triblock copolymer with grafted amphiphilic, nonionic Brij 78 side chain.

Dynamic Water Contact Angle Analysis. Dynamic water contact angles of the SABCs grafted with various amphiphilic, nonionic Brij side chains are summarized in Table 3. Both the SEBS and K3 control surfaces are highly hydrophobic with advancing contact angles of 119.8° and 115.9° respectively and receding contact angles of 59.8°and 57.6°. The SABC surfaces with grafted amphiphilic, nonionic Brij side chains have advancing contact angles ranging from 107.9° to 84.1° and receding contact angles in the range from 28.7° to 16.9°. The large difference between the advancing and receding contact angles corresponds to a large contact angle hysteresis. As the length of the PEG unit increased, the advancing contact angles decreased from 109.6° for the SABCs with grafted Brij 72 to 84.1° for the SABCs with grafted Brij 78. Simultaneously, the receding contact angles decreased slightly from 26.6° to 16.9°. High contact angle hysteresis was seen for all these surfaces, suggesting that surface reorganization of the backbone and side chain segments to expose the hydrated, hydrophilic PEG groups to a water environment at the surface occurs easily.

X-ray Photoelectron Spectroscopy (XPS). All SABCs showed a strong intensity peak from C═C and C−C near 285 eV, most likely indicative of a combination of the polymer backbone and the low surface energy aliphatic section of the nonionic derived side chain. Additionally, a pronounced shoulder at ca. ∼287 eV indicative of C−O suggests the presence of the PEG moieties of the nonionic side chain near the surface.

Figure 2 shows high-resolution C 1s and survey XPS spectra of the amphiphilic SABC derived from the PS_{8K}-*b*-$P(E/B)_{25K}$-*b*-PI_{10K} precursor with attached nonionic Brij 78 side chains taken at two different electron emission angles (0° and 75°) relative to the surface normal. At these energies the 3.2 nm photoelectron inelastic mean free path[32,48] gives sampling depths, *d*, of 3.2 and 0.8 nm at 0° and 75°, respectively. The high resolution spectra are normalized so that the total area under the carbon peaks is equal to unity. The SABCs with grafted amphiphilic, nonionic Brij 78 side chain showed a strong intensity peak from C−C near 285 eV, most likely indicative of a combination of the polymer backbone and the low surface energy aliphatic section of the Brij 78 derived side chain. Additionally, a pronounced shoulder at ca. ∼287 eV associated with C−O, suggesting the presence of the PEG moieties of the Brij 78 side chain, is observed near the surface. Analysis of the XPS survey scans given in Figure 2 show the surfaces dominated by the peaks associated with C 1s and O 1s, located at ca. ∼285 eV and ca. ∼535 eV respectively.

Near Edge X-ray Absorption Fine Structure (NEXAFS). Figure 3 depicts the normalized C 1s NEXAFS spectra of spray-coated surfaces of amphiphilic SABC derived from the PS_{8K}-*b*-$P(E/B)_{25K}$-*b*-PI_{10K} precursor with attached nonionic Brij 78 side chain taken at an angle from 20° to 125° between the surface and the soft X-ray beam. The sharp resonance peak near 288 eV can be attributed to the C 1s → σ^*_{C-H} signal. This peak indicates a surface dominated by the low surface energy

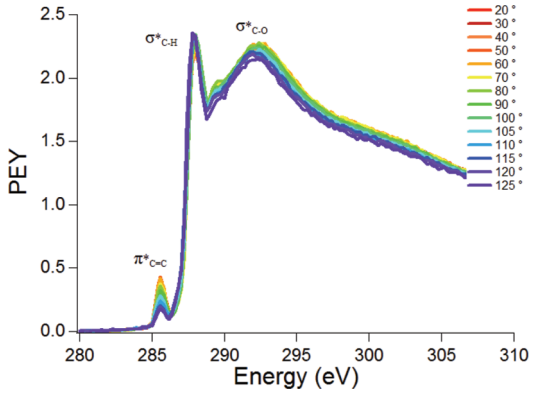

Figure 3. NEXAFS spectra of the triblock copolymer with grafted amphiphilic, nonionic Brij 78 side chain.

poly(ethylene-*ran*-butylene) block, with possible contributions from the aliphatic and PEG moieties. The characteristic signals near 293 eV can be easily seen for this triblock copolymer, and they are indicative of the C 1s $\rightarrow \sigma^*_{C-O}$ resonances, demonstrating the presence of the PEG containing side chains groups on the surfaces.[49,50] While the characteristic C 1s $\rightarrow \pi^*_{C=C}$ signals derived from the polystyrene block were observed near 285.5 eV, but the intensity of this peak was very low relative to what it would be for a pure PS surface, as expected since the other blocks of the SABC dominate the surface. All other SABCs show similar spectra to those shown in Figure 3 for the SABC with grafted amphiphilic nonionic Brij 78 side chains in NEXAFS analysis.

Atomic Force Microscopy (AFM). To characterize the behaviors of the surfaces in an aqueous environment, the surfaces were immerged in water for 7 days. Figure 4 shows the AFM phase images of a surface of the triblock copolymers with grafted Brij 72 side chain (A) and Brij 76 side chain (B) after dry annealing, and the triblock copolymers with grafted Brij 72 side chain (C) and Brij 76 side chain (D) after 7 days of immersion under water. The surfaces after annealing at 120 °C for 12 h (Figure 4, parts A and B) reveal mostly lying-down cylinders. However, this morphology was changed on exposure to water (Figure 4, parts C and D). The size of the detected domains on Brij 72 based surfaces ranges from 28 to 50 nm to 30−60 nm after immersion in water. In contrast the size of the domains on a Brij 76 based surface ranges from 33 to 50 nm to 40−150 nm. The size of the domains upon immersion in water increases in comparison to that observed during dry annealing. This result can be ascribed to the swelling of the hydrophilic PEG groups in water. It is noteworthy that the triblock copolymer with graft Brij 76 side chain containing a longer 10 unit hydrophiphilic PEG chains shows a greater change under water than does the triblock copolymer with grafted Brij 72 side chains that have only 2 PEG units.

Settlement of *Ulva* Spores and Release of *Ulva* Sporelings. Figure 5 shows the settlement density of *Ulva* spores on PDMS, SEBS and amphiphilic SABCs derived from the PS_{8K}-*b*-$P(E/B)_{25K}$-*b*-PI_{10K} precursor and Brij 56, Tergitol NP-9, or Silwet L-408 nonionic side chains. For the experimental coatings, the lowest settlement was shown on the surface incorporating the Brij 56 nonionic side chain. *Ulva* spores are known to preferentially settle on hydrophobic, low energy surfaces.[45] This was true for the PDMS standard surface, which showed the greatest settlement of *Ulva* spores. Dynamic water contact angle analysis

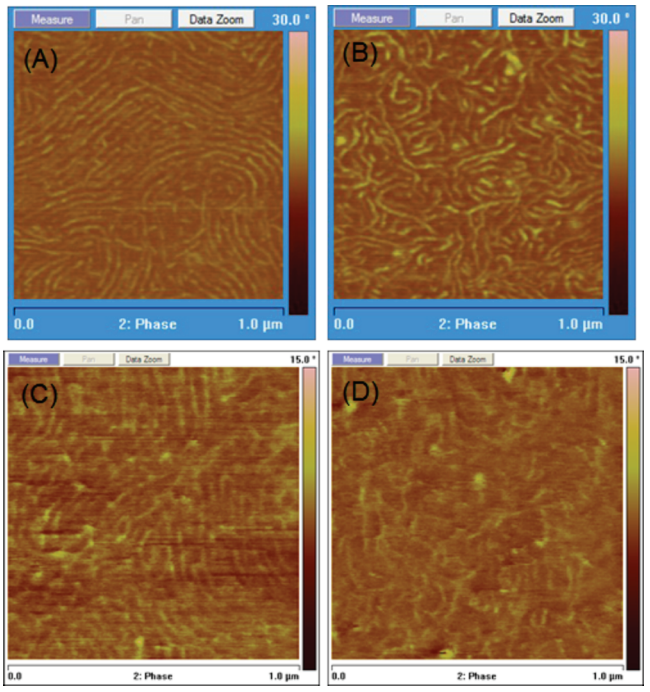

Figure 4. AFM phase images of the triblock copolymers with grafted Brij 72 side chain (A) and Brij 76 side chain (B) after dry annealing at 120 °C for 12 h; AFM phase images of the triblock copolymers with grafted Brij 72 side chain (C) and Brij 76 side chain (D) after 7 days of immersion under water.

indicated that all three nonionic surfactant derived SABCs had similar advancing and receding water contact angles, indicating a hydrophobic surface in a nonpolar environment, that was capable of reordering and becoming hydrophilic once placed in a polar environment such as water. Spore settlement density was dependent on the type of nonionic surfactant incorporated in the SABC coating however despite the similar water contact angles of all three samples. Settlement of *Ulva* spores was minimized on the Brij 56 derived SABC, with greatest settlement observed on the Tergitol NP-9 derived SABC. The SABC derived from Silwet L-408 showed a settlement density intermediate between the two other coatings. This clearly indicates that factors beyond wettability and contact angle hysteresis played a significant role in moderating spore settlement.

The biomass of sporelings, depicted in Figure 5B, largely reflected the number of spores settled. The percentage removal of sporelings from the experimental coatings at a range of applied water jet pressures is shown in Figure 5C. Sporelings were removed from the PDMS standard at low water jet pressures reflecting the good fouling-release characteristics of this low surface energy elastomer.[30,51] More remarkable however was the extreme difference in fouling release observed for the Brij 56 derived multilayer SABC coating compared to those derived from Silwet L-408 and Tergitol NP-9.

The SABC derived from the Brij 56 nonionic surfactant demonstrated higher release of *Ulva* sporelings than the PDMS standard. The coatings derived from both Silwet L-408 and Tergitol NP-9 meanwhile demonstrated removal only on the order of the SEBS control, indicating that these two experimental coatings did not function as effective fouling-release materials with regards to *Ulva* sporelings. This observation, when taken in conjunction with the settlement results for these coatings, clearly

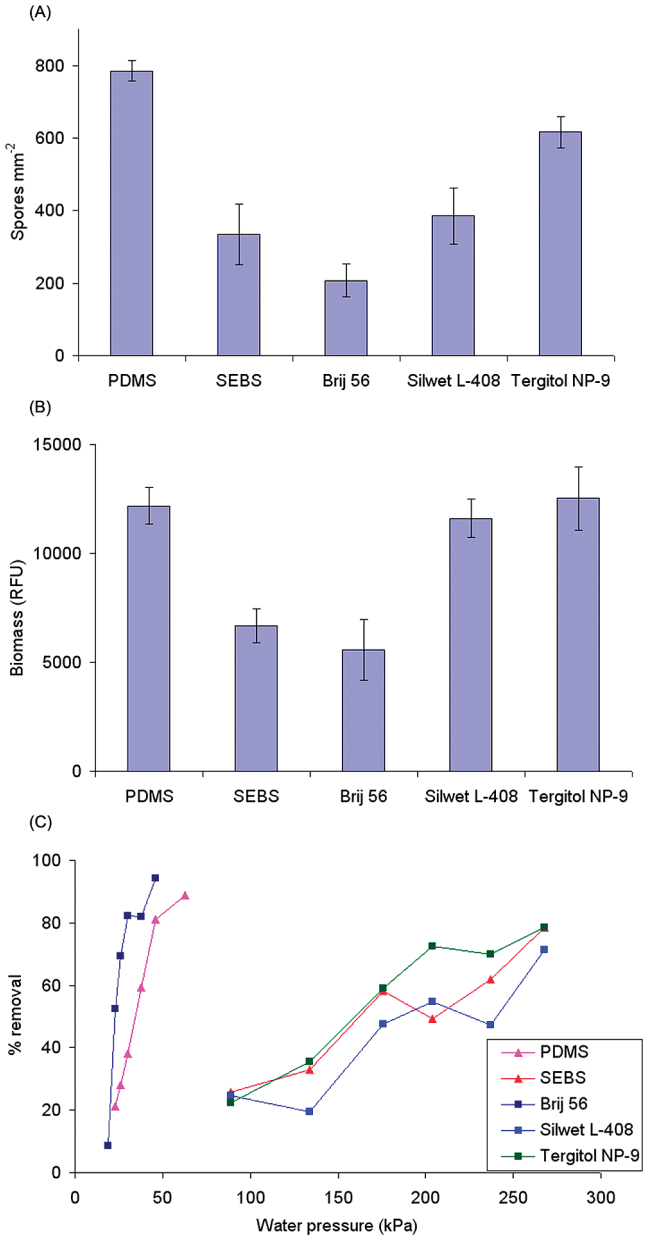

Figure 5. (A) Settlement of *Ulva* spores on SEBS, PDMS and PS_{8K}-*b*-$P(E/B)_{25K}$-*b*-PI_{10K} nonionic surfactant derived amphiphilic SABCs. Each point is the mean from 90 counts on 3 replicate slides. Bars show 95% confidence limits. (B) Biomass of *Ulva* sporelings on SEBS, PDMS and PS_{8K}-*b*-$P(E/B)_{25K}$-*b*-PI_{10K} nonionic surfactant derived amphiphilic SABCs. Each point is the mean biomass from 6 replicate slides measured using a fluorescence plate reader. Bars show standard error of the mean. (C) Removal of *Ulva* sporelings at a range of surface impact pressures from SEBS, PDMS and PS_{8K}-*b*-$P(E/B)_{25K}$-*b*-PI_{10K} nonionic surfactant derived amphiphilic SABCs.

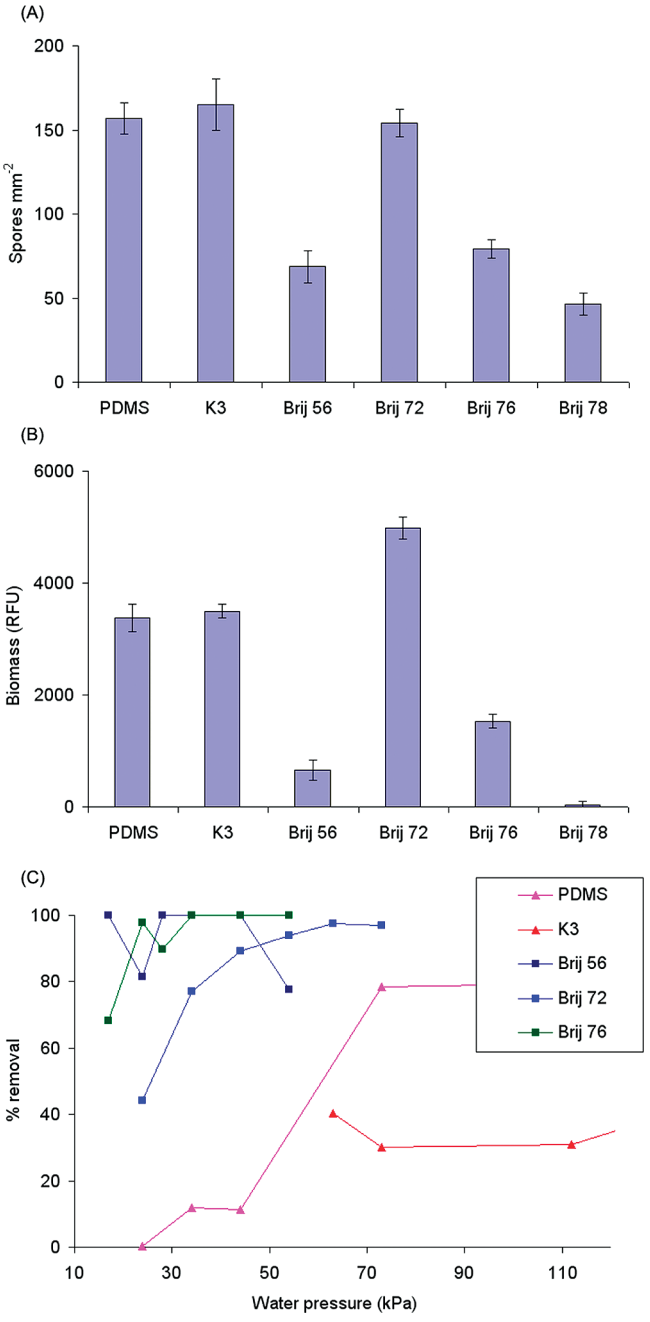

Figure 6. The settlement densities of *Ulva* spores on Brij nonionic side chain derived SABC surfaces (A). Biomass of *Ulva* sporelings on nonionic Brij derived SABC surfaces after 7 days (B). Detachment of *Ulva* sporelings from nonionic Brij derived SABC surfaces (C) as a function of water impact pressure.

indicates that the nonionic side chain structure appears to have a much greater effect on fouling-release behavior than simply altering surface wettability parameters. These initial results suggest that additional study using a range of Brij nonionic side chains incorporating different ratios of PEG and hydrocarbon moieties may lead to further improvement. Furthermore, the data suggest that excellent fouling-release behavior for amphiphilic materials can be realized in fluorine free systems.

Brij nonionic side chains incorporating different ratios of PEG and hydrocarbon moieties were synthesized (Table 2) and tested systematically with *Ulva*. These preliminary results suggested that Brij 72 (2 PEG units), 76 (10 PEG units), and 78 (20 PEG units) nonionic side chains incorporating different ratios of PEG and same length of hydrocarbon moieties are potential candidates as antifouling and fouling-release materials for *Ulva*. The Brij 56 that performed well in the preliminary tests has 16 rather than 18 carbons in the alkane portion and 10 PEG units. Figure 6 shows the settlement density of *Ulva* spores (A), biomass (B),

dx.doi.org/10.1021/ma200269s |*Macromolecules* 2011, 44, 4783–4792

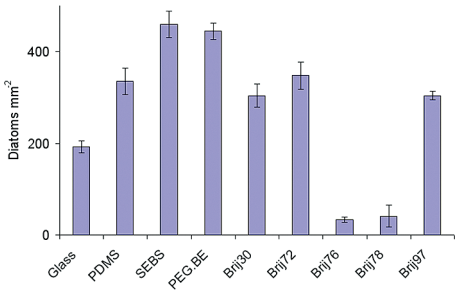

Figure 7. Density of attached *Navicula* cells on Brij nonionic side chain-derived SABC surfaces after exposure to a shear stress of 52 Pa in a water channel.

and detachment at a range of impact pressures (C) of *Ulva* sporeling on PDMS, PS_{8K}-*b*-$P(E/B)_{25K}$-*b*-PI_{10K} precursor (K3) and amphiphilic SABCs derived from the PS_{8K}-*b*-$P(E/B)_{25K}$-*b*-PI_{10K} precursor and the best Brij nonionic side chains. For the best Brij side chain coatings, the lowest settlement was shown on the surface incorporating the Brij 78 nonionic side chain. The growth of *Ulva* sporelings, depicted in Figure 6B, showed a similar trend with the density of settled spores. The percentage removal of *Ulva* sporelings from the experimental coatings is shown in Figure 6C. Sporelings were removed from the Brij-derived multilayer SABC coatings at low water jet pressures. Antifouling and fouling-release properties were found to depend on the length of the hydrophilic PEG units. The removal of sporelings from the Brij 78 derived SABC coating could not be tested because there was insufficient biomass on the surface. However, microscopic examination showed that the sporelings were healthy, so we conclude that the low biomass on the Brij 78 (and Brij 56) derived SABC was a consequence of low number of spores settled, rather than toxicity. We expect that the Brij 78-derived SABC coating that has the higher PEG content studied will provide the best surface for antifouling and fouling-release applications.

Attachment and Adhesion Strength of the Cells of the Diatom *Navicula*. Unlike *Ulva* spores that are motile and therefore able to "select" where to settle, diatom cells are not motile in the water column and reach a surface through transport in currents and gravity. In laboratory assays, the cells sink rapidly and form an even covering on the test surfaces. Any differences in the number of cells attached after gentle washing indicates their ability to adhere to a particular surface. A flow channel measures how strongly the cells adhere to a surface. Figure 7 shows the density of attached *Navicula* cells on Brij nonionic side chain derived SABC coating surfaces after exposure to a shear stress of 52 Pa. Data are presented for SABCs derived from the PS_{8K}-*b*-$P(E/B)_{25K}$-*b*-PI_{10K} precursor, the MD6945 SEBS and PDMS (Silastic T2). Figure 7 shows there was a decrease in the number of cells attached as the content of PEG in the side chains increased. These results show that diatom cells attached less strongly to the hydrophilic surfaces as shown for other types of coatings.[52] Diatom cells were attached most strongly to the hydrophobic PDMS and SEBS surfaces. In particular, Brij 76- and 78-derived SABC coatings are the best surfaces for minimizing the adhesion of diatom cells. The Brij 76 side chains with only 10 PEG units however show lower adhesion than the more hydrophilic Brij 78 side chains with 20 PEG units. Overall, Brij 76- and 78-derived SABC coatings should both be considered excellent surfaces for minimizing the adhesion of diatom cells.

CONCLUSIONS

Potential coatings for marine antifouling and/or fouling-release applications were developed through chemical modification of a PS_{8K}-*b*-$P(E/B)_{25K}$-*b*-PI_{10K} triblock copolymer with fluorine-free, amphiphilic, nonionic side chains. Resultant SABCs were obtained through the grafting of these amphiphilic molecules, consisting of a low surface energy aliphatic containing group combined with a hydrophilic PEG group, to the polyisoprene block of the precursor polymer. The presence of the nonionic side chains on the surfaces of all these triblock copolymer coatings was demonstrated in our studies using dynamic water contact angle, AFM, XPS, and NEXAFS analysis. The SABC prepared from grafted nonionic Brij side chains showed both lower settlement and better fouling-release performance against the green alga *Ulva* and cells of the diatom *Navicula* than the PDMS standard. The effectiveness of this coating that combines nonpolar hydrocarbon and PEG is consistent with our earlier observation that nonpolar fluorinated segments combined with PEG segments makes broadly effective antifouling coatings.[34] This suggests that despite similarities in wettability based on dynamic water contact angles, the chemical structure and/or surface chemistry present for the different nonionic side chains played a much more significant role in both deterring the settlement and encouraging the release of fouling organisms. Antifouling and fouling-release properties were found to depend on the length of the hydrophilic PEG units on Brij-derived SABC surfaces. Finally, it has been demonstrated that the fluorine-free, amphiphilic, nonionic Brij side chain-derived SABCs are good candidates for marine antifouling and fouling-release coatings as well as showing reduced potential environmental impact compared to fluorinated counterparts.

ACKNOWLEDGMENT

This work was supported by the Office of Naval Research (ONR) through Award No. N00014-02-1-0170 (C.K.O. and E.J.K.) and No. N00014-08-1-0010 (J.A.C. and M.E.C.). Additional support was provided by the United States Department of Defense's Strategic Environmental Research and Development Program (SERDP), Grant WP #1454. Additionally, E.J.K. and M.D. acknowledge partial support from the NSF Polymers Program (DMR-0704539) as well as the use of central facilities funded by the NSF-MRSEC program (UCSB MRL, DMR-0520415).

REFERENCES

(1) Schultz, M. P.; Bendick, J. A.; Holm, E. R.; Hertel, W. M. *Biofouling* **2011**, *27*, 87–98.
(2) Tribou, M.; Swain, G. *Biofouling* **2010**, *26*, 47–56.
(3) Finnie, A., Williams, D. N. In *Paint and Coatings Technology for the Control of Marine Fouling in Biofouling*; Durr, S., Thomason, J. C., Eds.; Wiley-Blackwell: Chichester, U.K., 2010; p 429.
(4) Thomas, K. V.; Brooks, S. *Biofouling* **2010**, *26*, 73–88.
(5) Yebra, D. M.; Kiil, S.; Dam-Johansen, K. *Prog. Org. Coat.* **2004**, *50*, 75–104.
(6) Genzer, J.; Efimenko, K. *Biofouling* **2006**, *22*, 339–360.
(7) Chambers, L. D.; Stokes, K. R.; Walsh, F. C.; Wood, R. J. K. *Surf. Coat. Technol.* **2006**, *201*, 3642–3652.
(8) Vladkova, T. *J. Univ. Chem. Technol. Metall.* **2007**, *42*, 239–256.
(9) Werner, C.; Maitz, M. F.; Sperling, C. *J. Mater. Chem.* **2007**, *17*, 3376–3387.
(10) Wisniewski, N.; Reichert, M. *Colloids Surf., B* **2000**, *18*, 197–219.
(11) Otsuka, H.; Nagasaki, Y.; Kataoka, K. *Adv. Drug Delivery Rev.* **2003**, *55*, 403–419.

(12) Harris, J. M.; Chess, R. B. *Nature Rev. Drug Discovery* **2003**, *2*, 214–221.
(13) Chen, S.; Jiang, S. *Adv. Mater.* **2008**, *20*, 335–338.
(14) Krishnan, S.; Weinman, C. J.; Ober, C. K. *J. Mater. Chem.* **2008**, *18*, 3405–3413.
(15) Beigbeder, A.; Degee, P.; Conlan, S. L.; Mutton, R. J.; Clare, A. S.; Pettitt, M. E.; Callow, M. E.; Callow, J. A.; Dubois, P. *Biofouling* **2008**, *24*, 291–302.
(16) Wynne, K. J.; Swain, G. W.; Fox, R. B.; Bullock, S.; Ulik, J. *Biofouling* **2000**, *16*, 277–288.
(17) Brady, R. F. *Polym. Paint Colour J.* **2000**, *190*, 18–20.
(18) Marabotti, I.; Morelli, A.; Orsini, L. M.; Martinelli, E.; Galli, G.; Chiellini, E.; Lien, E. M.; Pettitt, M. E.; Callow, J. A.; Conlan, S. L.; Mutton, R. J.; Clare, A. S.; Kocijan, A.; Donik, C.; Jenko, M. *Biofouling* **2009**, *25*, 481–493.
(19) Sommer, S.; Ekin, A.; Webster, D. C.; Stafslien, S.; Daniels, J.; Van Der Wal, L. J.; Thompson, S. E. Y.; Callow, M. E.; Callow, J. A. *Biofouling* **2010**, *26*, 961–972.
(20) Magin, C. M.; Long, C. J.; Cooper, S. P.; Ista, L. K.; Lopez, G. P.; Brennan, A. B. *Biofouling* **2010**, *26*, 719–727.
(21) Yarbrough, J. C.; Rolland, J. P.; DeSimone, J. M.; Callow, M. E.; Finlay, J. A.; Callow, J. A. *Macromolecules* **2006**, *39*, 2521–2528. Youngblood, J. P.; Andruzzi, L.; Ober, C. K.; Hexemer, A.; Kramer, E. J.; Callow, J. A.; Finlay, J. A.; Callow, M. E. *Biofouling* **2003**, *19*, 91–98.
(22) Grozea, C. M.; Walker, G. C. *Soft Matter* **2009**, *5*, 4088–4100.
(23) Prime, K. L.; Whitesides, G. M. *J. Am. Chem. Soc.* **1993**, *115*, 10714–10721.
(24) Ma, H.; Hyun, J.; Stiller, P.; Chilkoti, A. *Adv. Mater.* **2004**, *16*, 338–341.
(25) Schilp, S.; Kueller, A.; Rosenhahn, A.; Grunze, M.; Pettitt, M. E.; Callow, M. E.; Callow, J. A. *Biointerphases* **2007**, *2*, 143–150.
(26) Kitano, H.; Kawasaki, A.; Kawasaki, H.; Morokoshi, S. *J. Colloid Interface Sci.* **2005**, *282*, 340–348.
(27) Zhang, Z.; Chao, T.; Chen, S.; Jiang, S. *Langmuir* **2006**, *22*, 10072–10077.
(28) Aldred, N.; Li, G.; Gao, Y.; Clare, A. S.; Jiang, S. *Biofouling* **2010**, *26*, 673–683.
(29) Zhang, Z.; Finlay, J. A.; Wang, L.; Gao, Y.; Callow, J. A.; Callow, M. E.; Jiang, S. *Langmuir* **2009**, *25*, 13516–13521.
(30) Krishnan, S.; Wang, N.; Ober, C. K.; Finlay, J. A.; Callow, M. E.; Callow, J. A.; Hexemer, A.; Sohn, K. E.; Kramer, E. J.; Fischer, D. A. *Biomacromolecules* **2006**, *7*, 1449–1462.
(31) Gudipati, C. S. F.; Callow, J. A.; Callow, M. E.; Wooley, K. L. *Langmuir* **2005**, *21*, 3044–3053.
(32) Krishnan, S.; Ayothi, R.; Hexemer, A.; Finlay, J. A.; Sohn, K. E.; Perry, R.; Ober, C. K.; Kramer, E. J.; Callow, M. E.; Callow, J. A.; Fischer, D. A. *Langmuir* **2006**, *22*, 5075–5086.
(33) Park, D.; Weinman, C. J.; Finlay, J. A.; Fletcher, B. R.; Paik, M. Y.; Sundaram, H. S.; Dimitriou, M. D.; Sohn, K. E.; Callow, M. E.; Callow, J. A.; Handlin, D. L.; Willis, C. L.; Fisher, D. A.; Kramer, E. J.; C. K. Ober, C. K. *Langmuir* **2010**, *26*, 9772–9781.
(34) Weinman, C. J.; Finlay, J. A.; Park, D.; Paik, M. Y.; Krishnan, S.; Sundaram, H. S.; Dimitriou, M.; Sohn, K. E.; Callow, M. E.; Callow, J. A.; Handlin, D. L.; Willis, C. L.; Kramer, E. J.; C. K. Ober, C. K. *Langmuir* **2009**, *25*, 12266–12274.
(35) Martinelli, E.; Agostini, S.; Galli, G.; Chiellini, E.; Glisenti, A.; Pettiitt, M. E.; Callow, M. E.; Callow, J. A.; Graf, K.; Bartels, F. W. *Langmuir* **2008**, *24*, 13138–13147.
(36) Kannan, K.; Koistinen, J.; Beckmen, K.; Evans, T.; Gorzelany, J. F.; Hansen, K. J.; Jones, O. P. D.; Helle, E.; Nyman, M.; Giesy, J. P. *Environ. Sci. Technol.* **2001**, *35*, 1593–1598.
(37) Martin, J. W.; Mabury, S. A.; Solomon, K. R.; Muir, D. C. G. *Environ. Toxicol. Chem.* **2003**, *22*, 196–204.
(38) Genzer, J.; Sivaniah, E.; Kramer, E. J.; Wang, J. G.; Korner, H.; Xiang, M. L.; Char, K.; Ober, C. K.; DeKoven, B. M.; Bubeck, R. A.; Chaudhury, M. K.; Sambasivan, S.; Fischer, D. A. *Macromolecules* **2000**, *33*, 1882–1887.
(39) Xiang, M. L.; Li, X. F.; Ober, C. K.; Char, K.; Genzer, J.; Sivaniah, E.; Kramer, E. J.; Fischer, D. A. *Macromolecules* **2000**, *33*, 6106–6119.
(40) Sohn, K. E.; Dimitriou, M. D.; Genzer, J.; Fischer, D. A.; Hawker, C. J.; Kramer, E. J. *Langmuir* **2009**, *25*, 6341–6348.
(41) Krishnan, S.; Ward, R. J.; Hexemer, A.; Sohn, K. E.; Lee, K. L.; Angert, E. R.; Fischer, D. A.; Kramer, E. J.; C. K. Ober, C. K. *Langmuir* **2006**, *22*, 11255–11266.
(42) Schumacher, J. F.; Carman, M. L.; Estes, T. G.; Feinberg, A. W.; Wilson, L. H.; Callow, M. E.; Callow, J. A.; Finlay, J. A.; Brennan, A. B. *Biofouling* **2007**, *23*, 55–62.
(43) Callow, M. E.; Callow, J. A.; Pickett-Heaps, J. D.; Wetherbee, R. *J. Phycol.* **1997**, *33*, 938–947.
(44) Callow, M. E.; Jennings, A. R.; Brennan, A. B.; Seegert, C. E.; Gibson, A.; Wilson, L.; Feinberg, A.; Baney, R.; Callow, J. A. *Biofouling* **2002**, *18*, 237–245.
(45) Chaudhury, M. K.; Finlay, J. A.; Chung, J. Y.; Callow, M. E.; Callow, J. A. *Biofouling* **2005**, *21*, 41–48.
(46) Casse, F.; Ribeiro, E.; Ekin, A.; Webster, D. C.; Callow, J. A.; Callow, M. E. *Biofouling* **2007**, *23*, 267–276.
(47) Finlay, J. A.; Callow, M. E.; Schultz, M. P.; Swain, G. W.; Callow, J. A. *Biofouling* **2002**, *18*, 251–256.
(48) Cumpson, P. J. *Surf. Interface Anal.* **2001**, *31*, 23–34.
(49) Thomas, H. E.; Dean, M. D.; Michael, J. F. *Langmuir* **2007**, *23*, 3355–3362.
(50) Robert, J. K.; Daniel, A. F.; Joseph, L. L. *Langmuir* **2008**, *24*, 8187–8197.
(51) Finlay, J. A.; Krishnan, S.; Callow, M. E.; Callow, J. A.; Dong, R.; Asgill, N.; Wong, K.; Kramer, E. J.; Ober, C. K. *Langmuir* **2008**, *24*, 503–510.
(52) Finlay, J. A.; Bennett, S. M.; Brewer, L. H.; Sokolova, A.; Clay, G.; Gunari, N.; Meyer, A. E.; Walker, G. C.; Wendt, D. E.; Callow, M. E.; Callow, J. A.; Detty, M. R. *Biofouling* **2010**, *26*, 657–666.